THE EFFECT OF THE SPLIT NACA 0015 AIRFOIL ON VARIATIONS IN REYNOLDS NUMBER

Muhammad Fari Satria[1], James Julian[2*], Fitri Wahyuni[3], Waridho Iskandar[4]

[123]Teknik Mesin, Fakultas Teknik, Universitas Pembangunan Nasional Veteran Jakarta Jalan RS. Fatwamati Raya, Pd. Labu, Kec. Cilandak, Kota Depok, Jawa Barat, Indonesia
[4]Fluid Mechanics Laboratory, Universitas Indonesia, Kampus Baru UI, Depok 16424, Jawa Barat, Indonesia
**Corresponding author*: zames@upnvj.ac.id

Abstract

This research will discuss the advantages of a NACA 0015 airfoil with a split configuration under varying Reynolds numbers. Computational Fluid Dynamics (CFD) simulations with a K-epsilon turbulence model were conducted on a two-dimensional split airfoil to achieve this goal. Initially, simulations were carried out for the unsplit airfoil geometry at different Reynolds numbers within an angle of attack (AoA) range of 0^0 to 25^0. Subsequently, simulations were performed for the split airfoil geometry at various Reynolds numbers within the same AoA range. The unsplit airfoil experiences stall at AoA greater thCan 11^0 degrees, while the split airfoil experiences stall at AoA greater than 13^0 degrees. Additionally, using a split airfoil enhances C_l, with an average increase of approximately 7-8% across different Reynolds numbers. In addition to the C_l improvement, the split airfoil exhibits lower C_d values than the unsplit airfoil, with an average reduction of about 26-28% across all Reynolds number variations. Overall, using separate airfoils improves the aerodynamic performance of the airfoil, with an average increase in C_l/C_d of approximately 33-37% across all Reynolds number variations. In conclusion, the split airfoil performs better than the unsplit airfoil.

Keywords*: *CFD, NACA 0015, split airfoil

1. INTRODUCTION

An airfoil is a shape or geometry utilized in the cross-section of wings or wind turbine blades. The use of airfoils as wing components initially drew inspiration from the shape of bird wings and was adopted in aviation. Yan elucidates the relationship between lift force and the airflow around an aircraft wing, forming the theoretical foundation for wing design development [1]. As research progresses and aviation scenarios become more complex, The current demands exceed the dynamic capabilities of conventional wings. Aviation agencies worldwide have released multiple datasets related to airfoils, one of which is the set of airfoil profile data created by the National Advisory Committee for Aeronautics (NACA). This type of airfoil is currently the most commonly used. Airfoil innovation has expanded into various domains within fluid flow engineering in general. The characteristics of airfoil profiles are a crucial factor in wing design, as wing efficiency significantly relies on the shape of the airfoil profile employed. Therefore, several studies, such as airfoil shape optimization, have been conducted to explore airfoil profiles both through numerical and experimental approaches in the existing literature [2]

In conducting numerical simulations and experimental observations on the NACA 0015 airfoil profile, the numerical computations in this investigation indicate that stall phenomena manifest at an angle of attack of 16^0 degrees and a Reynolds number of 6.849 x 10^5. This leads to a reduction in the lift coefficient and an elevation in the drag coefficient [3]. They examined the NACA 4412 airfoil profile at a Reynolds number of 3×10^6. This study scrutinized the transition from laminar to turbulent flow utilizing two distinct numerical models: the k-epsilon model and the Spalart-Allmaras model. Subsequently, the numerical findings with experimental data revealed that the two numerical models yielded congruous outcomes when applied under high Reynolds number conditions [4].

DOI: http://dx.doi.org/10.24127/trb.v12i2.2845
Received 27 September 2023; Received in revised form 12 December 2023; Accepted 14 December 2023
Available online 31 December 2023

By introducing an additional Gurney flap to the NACA 0015 airfoil profile, they conducted a numerical evaluation of the performance of this modified configuration. Their findings show that the drag coefficient has not changed but there has been an increase in the force coefficient, so the design used is very profitable [5] . This study Shows that the double-split model is superior to the single-split model at AOA between 17^0 and 22^0, but in the range 0^0<AOA<17^0 the double-split model experiences a decline in performance compared to the single-split model. This decrease is due to two separation areas in the split channel of the double-split model, one near the inlet and the other at the sharp edge of the splitter [6].

Several studies have been conducted on the modification of the NACA 0015 airfoil, such as the addition of a Gurney flap, increasing the lift coefficient of the NACA 0015 airfoil. This indicates that the NACA 0015 profile still has some shortcomings, such as limited potential to generate maximum lift, early stall, suboptimal aerodynamic performance at low angles of attack, and significant drag. Split airfoil can be designed to reduce aerodynamic drag while simultaneously increasing lift. This study aims to optimize the design for the best combination of increased lift and reduced drag. Therefore, this research significantly enhances the aerodynamic performance of the NACA 0015 airfoil. The main objective of this research is to examine the influence of a split airfoil on the aerodynamic characteristics of the NACA 0015 wing profile at various Reynolds numbers of 1.6 x 10^6, 2 x 10^6, and 2.5 x 10^6 using Computational Fluid Dynamics (CFD) tools. Thus, the effects of the airfoil split can impact changes in the lift coefficient (C_l) and drag coefficient (C_d) and reveal the fluid flow characteristics around the airfoil.

2. METHOD

Geometry of the models

The geometry of the NACA 0015 airfoil profile was chosen, having no maximum camber, a camber position at 0%, and a thickness of 15%, with a chord length measuring 1000 mm. The split version was selected based on the best aerodynamic performance observed in the 2-D results from the previous study. [7]. The pressure surface near the stagnation point is chosen as the split point, which is at 90% of the chord length from the trailing edge. For comparison, on the suction surface a split exit point is selected at 40% of the trailing edge. The width of the split cut measures 1 cm. The 2-D split profile demonstration has a chord length (C) of 1 meter. The two-dimensional representation of both the NACA 0015 airfoil profile and the NACA 0015 split airfoil is depicted in Figure 1. [6]

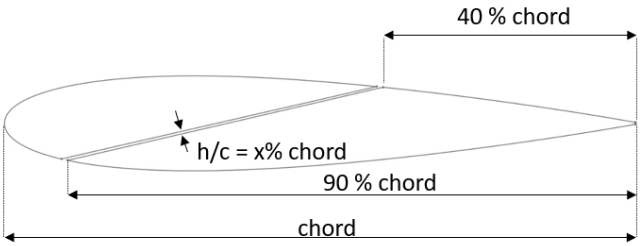

(a) NACA 0015 with split

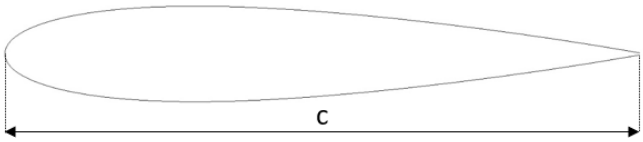

(b) Baseline NACA 0015

Figure 1. Geometry split airfoil and no split airfoil

Domain and boundary condition

This research, generated two distinct geometries, specifically, the fundamental NACA 0015 profile and the divided NACA 0015 profile. The airfoil possesses a chord length (c) of 1 meter. The study incorporates two distinct zones within the domain. The first section acts as the inlet for fluid velocity, while the second is the outlet for fluid pressure. An anti-slip boundary is established over the entire surface of the main airfoil profile. In contrast, for the airfoil experiencing flow separation, the

boundary condition applied to the divided region is characterized as a velocity inlet. The domain dimensions and boundary conditions are visualized in Figure 2.

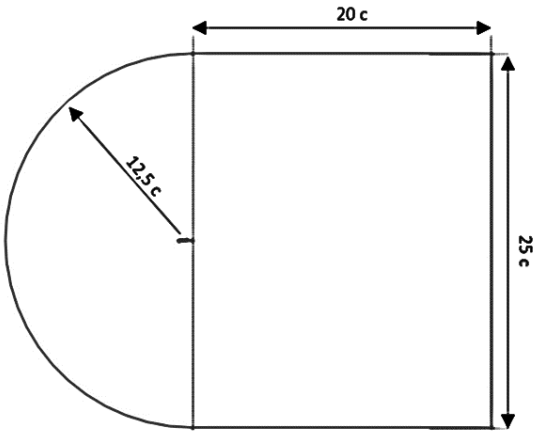

Figure 2. Fluid domain

Meshing

following the configuration of all geometry and subsequent computational steps. Meshing is defined as a computational step where the geometry of a domain is divided into smaller slices for computational purposes. Each segment in the net is called a net element. One category of mesh elements is rectangular elements, which are very suitable for structured meshes because their per-iteration cost is lower than other mesh elements. Another category is triangular meshing, which is highly adaptable, even to complex geometries, making it a common choice for unstructured meshing. This research proposes mesh variations of 25 x 103, 50 x 103, and 105. Mesh independence tests are carried out to evaluate these variations and identify the most efficient. Meshing options, which are then used for further computational procedures. The meshing approach used in this research is structured meshing. Next, each mesh element is placed near the airfoil surface so that the flow near the airfoil is captured.[8]. Additional information will be provided as depicted in Figure 3.

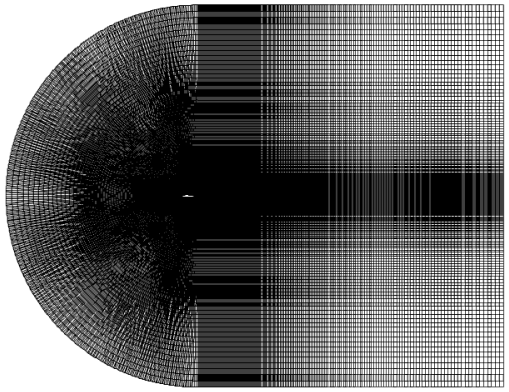

a. domain fine (100000 elements)

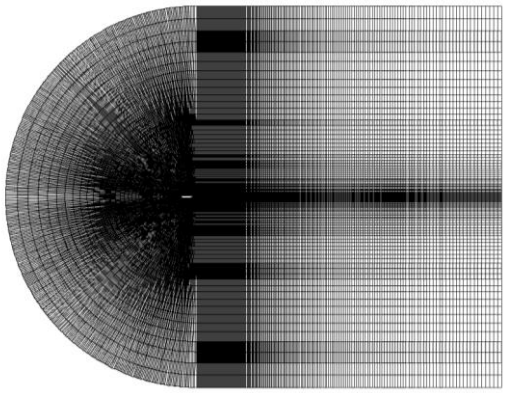

b. domain medium (50000 elements)

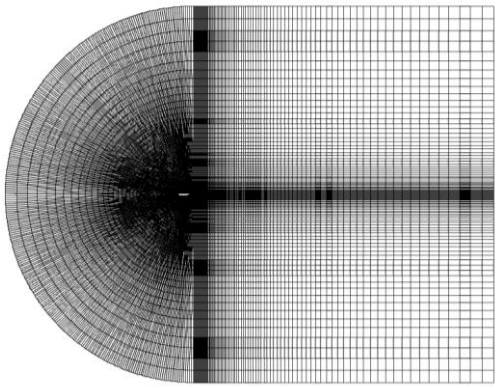

c. domain coarse (25000 elements)

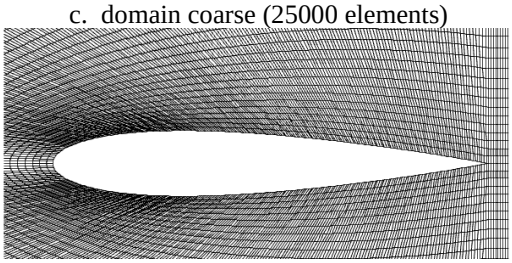

d. baseline NACA 0015

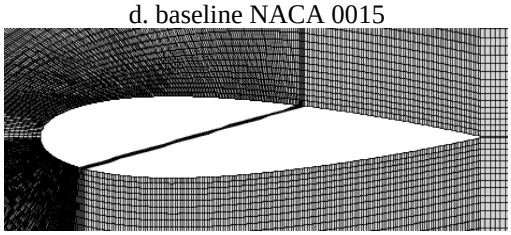

e. Naca 0015 split

Figure 3. Mesh

Governing equations

The primary equation introduced in this document is the Reynolds-Averaged Navier-Stokes equation (RANS). Mathematically, the RANS equation is detailed in equations 1 and 2 [9]The k-ε model is commonly employed in turbulence modeling methodology, being a widely used turbulence model in computational simulation. Equations 3 and 4 represent the mathematical expressions for the k-ε turbulence model. [10]. The selection of the k-ε equation in this study is based on its cost-effectiveness per iteration compared to the other two-equation turbulence models.

$$\frac{\partial \rho}{\partial t} + \frac{\partial}{\partial x_i}(\rho u_i) = 0 \quad (1)$$

$$\frac{\partial}{\partial t}(\rho u_i) + \frac{\partial}{\partial x_i}(\rho u_i u_j) = -\frac{\partial \rho}{\partial x_i} + \frac{\partial}{\partial x_j}\left[\mu\left(\frac{\partial u_j}{\partial x_i} + \frac{\partial u_i}{\partial x_j} - \frac{2}{3}\delta_{ij}\frac{\partial u_j}{\partial x_j}\right)\right] + \frac{\partial}{\partial x_j}\left(\rho\overline{\dot{u}_\iota\, \dot{u}_J}\right) \quad (2)$$

$$\frac{D}{D_t}(\rho k) = \frac{\partial}{\partial x_j}\left[\left(\mu + \frac{\mu_t}{\sigma_k}\right)\frac{\partial k}{\partial x_j}\right] + G_k - \rho\varepsilon \quad (3)$$

$$\frac{D}{D_t}(\rho \varepsilon) = \frac{\partial}{\partial x_j}\left[\left(\mu + \frac{\mu_t}{\sigma_\varepsilon}\right)\frac{\partial \varepsilon}{\partial x_j}\right] + C_{el}\frac{\varepsilon}{k}G_k - \rho C_{\varepsilon 2}\frac{\varepsilon^2}{k} \quad (4)$$

Aerodynamic of airfoil

Evaluating a split airfoil flow as a passive flow control primarily hinges on the airfoil's aerodynamics. Two commonly deliberated aerodynamic forces encompass the drag force and the lift force [11]. Drag force can also be called aerodynamic force which is oriented in the direction of fluid flow [12]. Meanwhile, Lift force can be called an aerodynamic force whose vector is perpendicular to the direction of fluid flow. for drag and lift forces with dimensionless values usually referred to as drag and lift coefficients. These values are sequentially mentioned in equations 5 and 6 [13]

$$C_d = \frac{d}{\frac{1}{2}\rho U^2 c} \quad (5)$$

$$C_l = \frac{l}{\frac{1}{2}\rho U^2 c} \quad (6)$$

3. RESULT AND DISCUSSIONS

In this research, it is imperative to analyze of mesh variations to ensure that all meshes fall within the specified convergence range. Furthermore, it is essential to calculate the error values for each mesh. There is a singular approach, known as the mesh independence test, which can concurrently achieve both of these objectives [14]. This method is known as Richardson Extrapolation, a concept expanded upon by Roache. Each phase of the mesh independence assessment is conducted following a methodology similar to that utilized in Julian's prior study [15]. The investigation mesh independence test included the measurement of velocity at coordinates x=0.5 and y=0.15 surrounding the airfoil. with a mesh refinement ratio of 2. In the mesh independence test, an order of accuracy of 1.8 was achieved. The calculated convergence index percentages for the refined and less refined meshes were 1.100% and 2.4948%, respectively. A safety factor of 1.25 was applied in the mesh independence test, resulting in a relative error of 0.0024. Ultimately, the outcome of the mesh independence test converged to a value of 1, indicating that mesh variations contributed to the convergence index. The parameter value obtained was 25.86624. In summary, this information is presented in Figure 4, and it is evident that the finer mesh provided the parameter value that closely matched the desired criteria, leading to its selection for subsequent calculations.

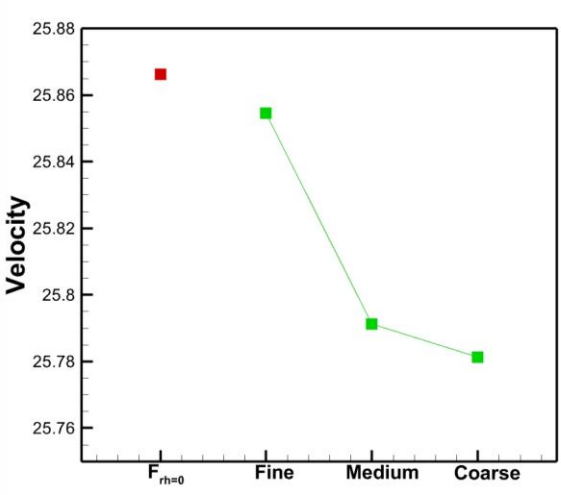

Figure 4. Mesh independence test

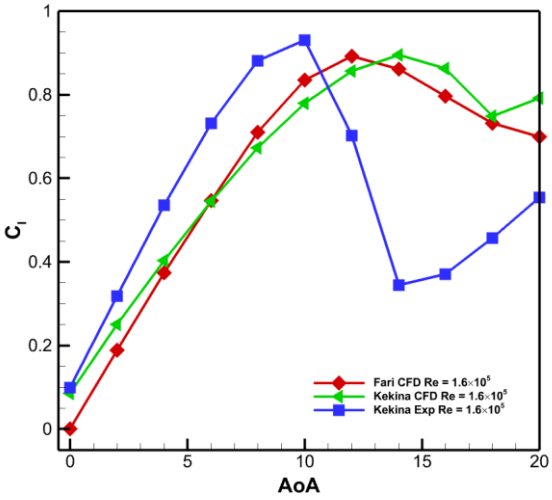

Figure 5. Validation C_l

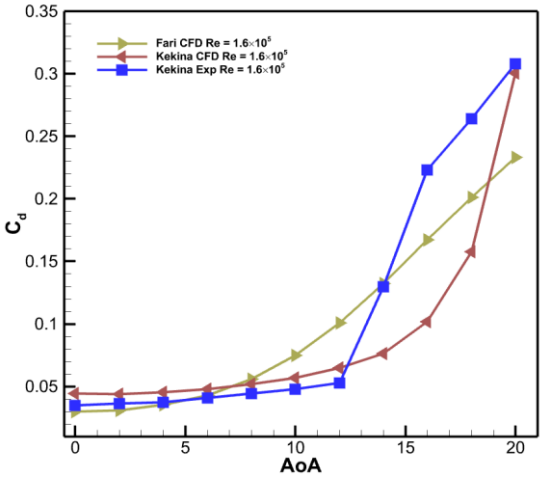

Figure 6. Validation C_d

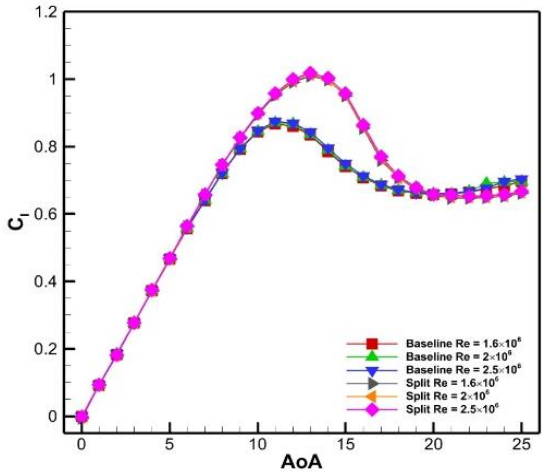

Figure 7. Koefisien lift

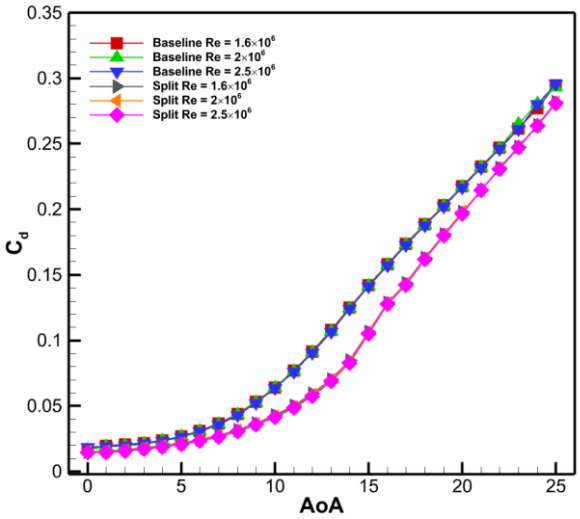

Figure 8. Koefisien drag

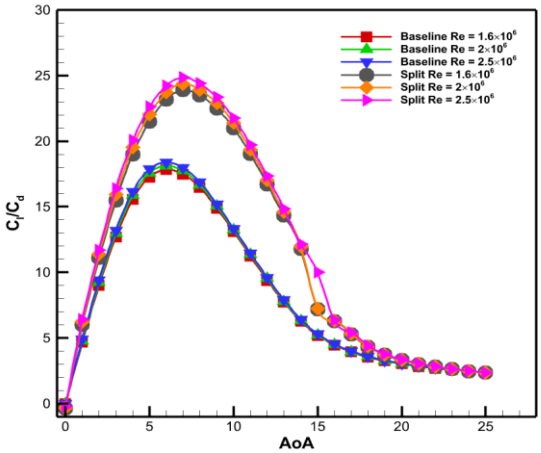

Figure 9. Comparasion C_l and C_d

The selected Reynolds number in this study is $1{,}6\times10^5$, calculated based on the airfoil's chord length. The aerodynamic data in this research, namely C_l and C_d, were analyzed in a two-dimensional form. The experimental data consists of C_l and C_d aerodynamic data from the original NACA 0015 profile, and research obtained from Kekina[16], which will be presented in Figure 5 and Figure 6. The C_l and C_d curves of Kekina Exp and Fari CFD exhibit similar trends. Both Kekina Exp and Fari CFD experience the same increase in C_l up to AoA 10^0. Furthermore, Kekina Exp and Fari CFD both show an increase in C_d as AoA increases. When AoA is less than 6^0, Kekina Exp has a higher C_d than Fari CFD, but after reaching AoA 6^0, Fari CFD's C_d becomes higher than Kekina Exp's until AoA 14^0. Then, Kekina Exp's Cd becomes higher than Fari CFD's again.

The data in this study were obtained from Computational Fluid Dynamics simulations on both the non-split airfoil and the split airfoil. Figure 7 illustrates that the curves for the non-split airfoil and the split airfoil exhibit the same trend. Both the non-split and split airfoils experience an increase in C_l with an increase in angle of attack up to a certain angle of attack. Beyond that AoA, the airfoil experiences a decrease in C_l, indicating a stall condition. Stall conditions for the non-split airfoil occur at AoA 12^0, while for the split airfoil, it occurs at AoA 14^0. This demonstrates that modifying the airfoil using a split can indeed delay stall. This phenomenon holds for all Reynolds number variations. Furthermore, the split in the airfoil also influences the increase in coefficient lift. This is evidenced by an average coefficient lift increase of 7% at various Reynolds numbers of 1,6 x 10^6 and 2 x 10^6 and 8% at various Reynolds numbers of 2,5 x 10^6. Therefore, it can be concluded that the use of a split in the airfoil can be advantageous from a C_l perspective. However, the magnitude of the C_l increase generated is not always the same across all Reynolds numbers.

In addition to increasing C_l, a split airfoil can also improve airfoil performance by reducing C_d. Figure 8 shows that the curves for the non-split airfoil and the split airfoil exhibit the same trend. Both the non-split and split airfoils experience an increase in C_d with an increase in AoA, but the value for the split airfoil is lower than that of the non-split airfoil. This is evidenced by an average Cd reduction of 26% at various Reynolds numbers of 1,6 x 10^6, 27% at various Reynolds numbers of 2 x 10^6, and 28% at various Reynolds numbers of 2,5 x 10^6. Following the stall, the escalation of C_d becomes more pronounced owing to the adverse separation of fluid flow transpiring on the upper surface of the airfoil, potentially resulting in elevated C_d values.. Fluid separation can increase C_d values because of the extreme pressure difference between the fluid flow before interacting with the airfoil and the separated flow. This extreme pressure difference causes the airfoil to experience rearward thrust. In the AoA range of 0° to 25°, the split airfoil can generate lower C_d values compared to the non-split airfoil. Further details on this will be discussed in the velocity and pressure contour analysis.

This figure 9 illustrates that both the non-split and split airfoils follow a similar trend in their curves. The highest point on the curve corresponds to the maximum angle of attack. For the non-split airfoil, the optimum angle of attack is attained at AoA = 6^0. Conversely, for the split airfoil, the optimal angle of attack is at AoA = 7^0, and the peak point on the curve for the split airfoil surpasses that of the non-split airfoil. This holds for all Reynolds number variations. This is due to the significantly greater C_l generated compared to C_d. Therefore, it can be deduced that the utilization of a split airfoil holds the potential to enhance the airfoil's overall aerodynamic efficiency. This is supported by an average increase in C_l/C_d of 33% at various Reynolds numbers of 1,6 x 10^6, 34% at various Reynolds numbesr of 2 x 10^6, and 37% at various Reynolds numbers of 2,5 x 10^6.

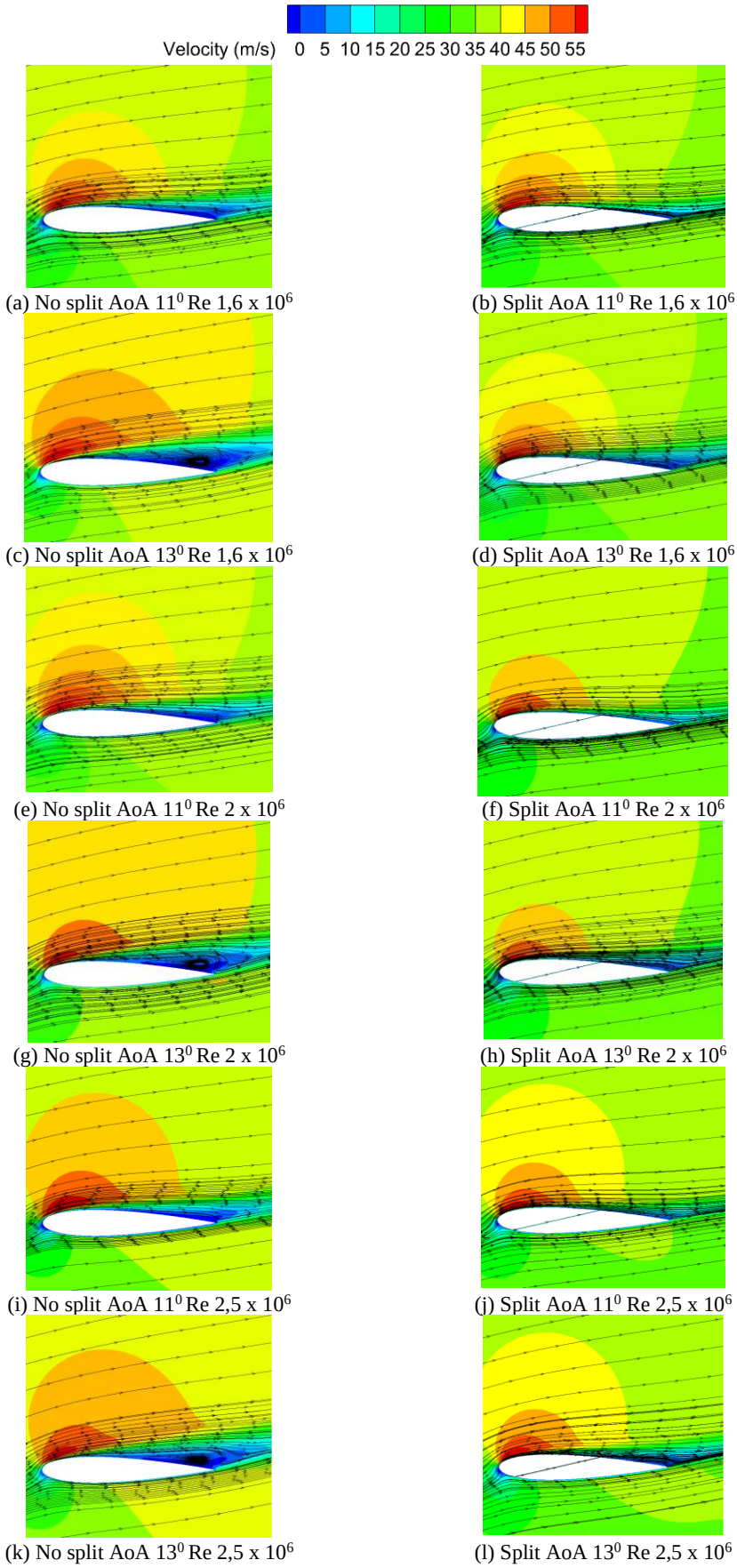

(a) No split AoA 11^0 Re 1,6 x 10^6 (b) Split AoA 11^0 Re 1,6 x 10^6

(c) No split AoA 13^0 Re 1,6 x 10^6 (d) Split AoA 13^0 Re 1,6 x 10^6

(e) No split AoA 11^0 Re 2 x 10^6 (f) Split AoA 11^0 Re 2 x 10^6

(g) No split AoA 13^0 Re 2 x 10^6 (h) Split AoA 13^0 Re 2 x 10^6

(i) No split AoA 11^0 Re 2,5 x 10^6 (j) Split AoA 11^0 Re 2,5 x 10^6

(k) No split AoA 13^0 Re 2,5 x 10^6 (l) Split AoA 13^0 Re 2,5 x 10^6

Figure 10. Velocity contour

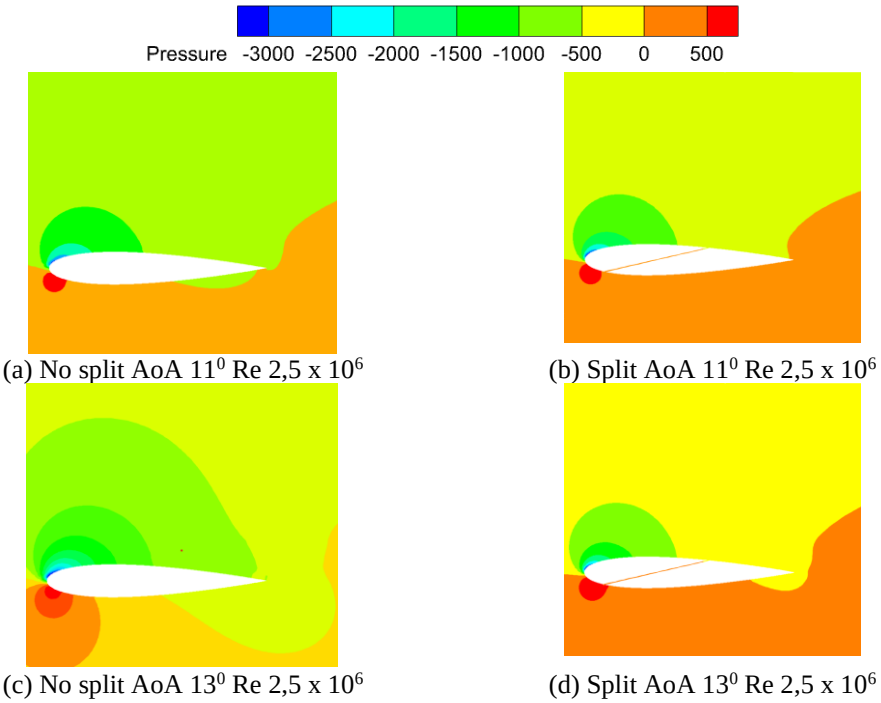

(a) No split AoA 11^0 Re 2,5 x 10^6 (b) Split AoA 11^0 Re 2,5 x 10^6

(c) No split AoA 13^0 Re 2,5 x 10^6 (d) Split AoA 13^0 Re 2,5 x 10^6

Figure 11. Pressure contour

The next visualization concerns the distribution of pressure on the airfoil. Fluid speed in the upper chamber can be increased, this is a characteristic of airfoils. An increase in fluid velocity causes a decrease in pressure, this is based on the Bernoulli principle. In other words, there exists an inverse relationship between fluid velocity and pressure. However, a velocity increase also manifests in the lower chamber. As a result, when AOA is 0^0 , the ability to produce lift is reduced. Figure 11 illustrates the pressure contours surrounding the airfoil at (AoA) of 11^0 and 13^0 degrees. The fluid pressure differential between the upper and lower chambers, as depicted in Figure 11, results in lift generation at these angles of attack (AoA). Separation of flow reduces pressure in the upper chamber, leading to alterations in pressure distribution in the lower chamber. Contrary to the upper chamber, changes in the lower chamber are such that increased fluid injection results in elevated pressure. Therefore, greater fluid flow injection correlates with higher lift coefficients (C_l) generated by the airfoil due to the greater pressure at the bottom of the airfoil which causes the airfoil to lift higher.

4. CONCLUSION

The C_l for the split airfoil and the non-split airfoil exhibit similar trends. Both experience an increase in C_l with increasing AoA until reaching a certain point. Afterward, there is a decrease in C_l, indicating that the airfoil is in a stall condition. The split airfoil shows a significant delay in stall compared to the non-split airfoil. In addition to improving C_l, the use of a split airfoil can also reduce C_d because the stall point in the split airfoil can be delayed until a certain AoA. The split airfoil has a lower C_d than the non-split airfoil at various Reynolds numbers. This study also determines the optimum AoA of the airfoil. The findings demonstrate that the split airfoil exhibits a superior optimal angle of attack (AoA) when compared to the non-split airfoil, and this trend persists across all variations of Reynolds numbers. This is due to the significant increase in C_l in the split airfoil. When looking at velocity visualization, it becomes evident that the split airfoil can control fluid flow in the upper chamber and reduce separation, which can help prevent stall. Pressure visualization around the airfoil also demonstrates that the

split airfoil can generate favorable pressure distributions, enabling lift generation at higher AoA. Thus, this research indicates that the use of a split airfoil can significantly enhance aerodynamic performance with increased C_l, reduced C_d, and an improved optimum AoA, which can have positive implications for various aerodynamic applications.

REFERENCE

[1] H. Yan *et al.*, "Design approach and hydrodynamic characteristics of a novel bionic airfoil," *Ocean Engineering*, vol. 216, Nov. 2020, doi: 10.1016/j.oceaneng.2020.108076.

[2] D. S. Miklosovic, M. M. Murray, L. E. Howle, and F. E. Fish, "Leading-edge tubercles delay stall on humpback whale (Megaptera novaeangliae) flippers," *Physics of Fluids*, vol. 16, no. 5, 2004, doi: 10.1063/1.1688341.

[3] İ. Şahin and A. Acir, "Numerical and Experimental Investigations of Lift and Drag Performances of NACA 0015 Wind Turbine Airfoil," *International Journal of Materials, Mechanics and Manufacturing*, vol. 3, no. 1, pp. 22–25, 2015, doi: 10.7763/ijmmm.2015.v3.159.

[4] Ravi H C, Madhukeshwara N, and S. Kumarappa, "NUMERICAL INVESTIGATION OF FLOW TRANSITION FOR NACA-4412 AIRFOIL USING COMPUTATIONAL FLUID DYNAMICS," *Int J Innov Res Sci Eng Technol*, vol. 2, 2013, [Online]. Available: www.ijirset.com

[5] D. R. Troolin, E. K. Longmire, and W. T. Lai, "Time resolved PIV analysis of flow over a NACA 0015 airfoil with Gurney flap," in *Experiments in Fluids*, Aug. 2006, pp. 241–254. doi: 10.1007/s00348-006-0143-8.

[6] M. Moshfeghi, M. Ramezani, and N. Hur, "Design and aerodynamic performance analysis of a finite span double-split S809 configuration for passive flow control in wind turbines and comparison with single-split geometries," *Journal of Wind Engineering and Industrial Aerodynamics*, vol. 214, Jul. 2021, doi: 10.1016/j.jweia.2021.104654.

[7] L. H. Hodges, W. Reichelderfer, J. E. Caskey, and E. Volume, "DEPARTMENT OF COMMERCE MONTHLY WEATHER REVIEW GENERAL CIRCULATION EXPERIMENTS WITH THE PRIMITIVE EQUATIONS I. THE BASIC EXPERIMENT* 100 MONTHLY WEATHER REVIEW CONTENTS," 1963.

[8] A. Choudhry, M. Arjomandi, and R. Kelso, "A study of long separation bubble on thick airfoils and its consequent effects," *Int J Heat Fluid Flow*, vol. 52, pp. 84–96, Apr. 2015, doi:10.1016/j.ijheatfluidflow.2014.12.001.

[9] S. M. A. Aftab, A. S. M. Rafie, N. A. Razak, and K. A. Ahmad, "Turbulence model selection for low reynolds number flows," *PLoS One*, vol. 11, no. 4, Apr. 2016, doi: 10.1371/journal.pone.0153755.

[10] A. J. Lew, G. C. Buscaglia, and P. M. Carrica, "A Note on the Numerical Treatment of the k-epsilon Turbulence Model," *Int J Comut Fluid Dyn*, vol. 14, no. 3, pp. 201–209, 2001, doi: 10.1080/10618560108940724.

[11] H. Harinaldi, B. Budiarso, J. Julian, and A. WS, "Drag Reduction in Flow Separation Using Plasma Actuator in a Cylinder Model," 2015.

[12] Harinaldi, M. D. Kesuma, R. Irwansyah, J. Julian, and A. Satyadharma, "Flow control with multi-DBD plasma actuator on a delta wing," *Evergreen*, vol. 7, no. 4, pp.

602–608, 2020, doi: 10.5109/4150513.
[13] J. Julian, W. Iskandar, and F. Wahyuni, “Effect of Single Slat and Double Slat on Aerodynamic Performance of NACA 4415,” 2022.
[14] J. Julian, W. Iskandar, and F. Wahyuni, “COMPUTATIONAL FLUID DYNAMICS ANALYSIS BASED ON THE FLUID FLOW SEPARATION POINT ON THE UPPER SIDE OF THE NACA 0015 AIRFOIL WITH THE COEFFICIENT OF FRICTION,” *Jurnal Media Mesin*, vol. 23, no. 2, 2022.
[15] J. Julian, W. Iskandar, F. Wahyuni, D. Nely, and T. Bunga, “Aerodynamic Performance Improvement on NACA 4415 Airfoil by Using Cavity Peningkatan Performa Aerodinamika NACA 4415 dengan Menggunakan Cavity Aerodynamic Performance Improvement on NACA 4415 Airfoil by Using Cavity,” vol. 5, pp. 135–142, 2023, doi: 10.35814/asiimetrik.v5i1.4259.
[16] P. Kekina and C. Suvanjumrat, “A Comparative Study on Turbulence Models for Simulation of Flow Past NACA 0015 Airfoil Using OpenFOAM,” 2016.